MedCrave
Step into the World of Research
International Journal of Radiology & Radiation Therapy

Research Article

Open Access

Development of silica containing samarium and iron oxide for cancer treatment by brachytherapy and magnetic hyperthermia

Abstract

The combinated therapy for cancer treatment aims to use methods that act through different mechanisms, reducing the probability of developing resistant cancer cells and intolerable side effects. The Magnetic hyperthermia is a modern, directional, and minimally invasive technique that is based on increasing the temperature of tumor cells by means of heat dissipated by particles (subjected) to an alternating magnetic field. Brachytherapy is an oncological treatment where a radioactive source is placed in or near the tumor area for localized treatment of the tumor cells. In this work, silica particles containing iron oxide and samarium (Si-Mag-Sm) were produced by the Sol-Gel method to act as agents for the combined treatment of cancer by hyperthermia and brachytherapy.

The iron oxides were characterized by Mössbauer, Zeta Potential, TEM and SEM, and magnetization measurements. The samples were characterized by FTIR, DRX, FRX and TG. The radioactive activity of the elements was estimated by a theoretical dosimetric calculation. XRD, FTIR and XRF techniques indicated synthesis of silica containing samarium and iron oxide. TG indicated loss of adsorbed water between 25 and 150°C, elimination of nitrates and condensation reactions between 160 and 700°C and residual mass of 90%. The dosimetric calculation outlined relevant activity for ^{153}Sm, being higher than the other elements. The morphology of the natural iron oxide observed by TEM showed properties suitable for use in cancer treatment. The Zeta potential showed that the iron oxide has excellent suspension properties for in vivo applications and by the Mössbauer technique, the iron oxide showed superparamagnetic behavior at room temperature.

Keywords: cancer, samarium, brachytherapy, hyperthermia, iron oxide

Volume 10 Issue 4 - 2023

Gabriela Veloso,[1] Roberta Ferreira,[1] Wanderley Roberto,[2] Sidney Nicodemos da Silva[2]

[1]Departamento de Engenharia de Materiais/Cefet-MG, 30.480-000, Av. Amazonas, 5253, Belo Horizonte, Minas Gerais, Brasil
[2]Departamento de Física/Cefet-MG, 30510-000, Av. Amazonas, 7675, Belo Horizonte, Minas Gerais, Brasil

Correspondence: Gabriela Veloso, CEFET-MG - Departamento de Engenharia de Materiais, Belo Horizonte – Minas Gerais – Brasil,
Email gabrielaveloso.engmateriai@gmail.com

Received: August 27, 2023 | **Published:** September 12, 2023

Introduction

Cancer is responsible for one of the highest mortality rates worldwide despite the efforts of research and the pharmaceutical industry to develop new drugs and treatments.

Cancer is responsible for one of the highest mortality rates worldwide despite the research´s efforts and the development of new drugs and treatments, by the pharmaceutical industry. Currently the most commonly used cancer treatment techniques consist of surgery, radiotherapy and chemotherapy. The neoplastic classification, staging, volume, location and the occurrence of metastases are examples of factors that influence the success of the treatment. Given the disadvantages and limitations of the conventionally used treatments, the investment in studies for combined treatments with higher assertiveness rates allied to the decreasing invasiveness of treatments is justified.[1-3]

One of the efficient and traditional methods for cancer treatment is brachytherapy. While in conventional radiotherapy, radiation is applied outside the body to an area where the tumor is located and may affect healthy cells. In brachytherapy radiation is applied through an implant inside the body. An implant of radioactive material is introduced into the tumor region after applying a high dose of local radiation to eliminate tumor cells while preserving the surrounding healthy tissue. The treatment decreases the risk of common side effects such as fatigue, redness, dryness and irritation of the skin, or hair loss, for example.[4]

The radioactive material of the implant, also called radioactive seed, is currently used in clinical applications. Its matrix is made of titanium filled with (iodine-125) ^{125}I. The efficiency of treatment by the chosen radionuclide, the required number of seeds, their size and dispersion in the organ, along with their permanence in the tumor are points requiring improvement. Other radionuclides may offer better conditions in the treatment. The rare earth element isotope (samarium-152) ^{152}Sm incorporated in ceramic matrix synthesized by the sol-gel route, can improve the form of treatment by brachytherapy and the seeds can be produced in suitable dimensions.[5-8] A recent study showed that the use of another rare earth element, holmium-166, in ceramic matrix can also be interesting for brachytherapy cancer treatment.[9]

The treatment of cancer by magnetic hyperthermia (MH) is based on the observation that tumor cells are less resistant to temperature increase when compared to a healthy cell. The treatment consists of scattering magnetic particles on the diseased tissue and then applying an alternating magnetic field of sufficient intensity and frequency to cause the particles to heat up. At temperatures around 41-42ºC there will be lysis of the tumor cells without damage to normal cells. This type of treatment has advantages over the destructive effects of conventional thermotherapy (41-45°C) on the plasma membrane, which can damage DNA, denature proteins, change the microenvironmental pH and induce apoptosis in tumor cells.[10] HM treatment can be applied individually or combined with conventional therapies. Currently several materials are studied in HM: metals, metal oxides, metal alloys, porous oxides and polymers.[11]

The iron oxides magnetite (Fe_3O_4) and maghemite (γ-Fe_2O_3) have been widely studied over the years as agents for HM treatment. They respond to an alternating magnetic field by dissipating heat

and are therefore excellent agents for hyperthermia.[12,13] In addition, a major advantage of iron oxide particles is that when they degrade in the physiological environment they release iron ions that can be incorporated into hemoglobin or utilized by conventional organic cycles, and are thus biocompatible. However, such particles are prone to aggregation and sedimentation, so it is important to surround the (magnetic) nanoparticles with a non-magnetic layer for *in vivo* applications.[14]

The present paper describes the preparation and characterization of silica particles containing iron oxide and samarium (Si-Mag-Sm) to act as agents for combined treatment of cancer by hyperthermia and brachytherapy.

Materials and methods

Preparation of the iron oxide samples

The natural iron oxide samples were obtained from the reuse of the ilmenite - $FeTiO_3$ mining extraction from titania – TiO_2 (Vale) and were supplied by the company Phosther Inovações (Santa Luzia/MG). The material was reprocessed to remove impurities, undergoing comminution in a ball mill and sieved below 400 mesh.

The samples produced in this work were: Silica containing Iron Oxide (Si-Mag), and Silica containing Iron Oxide and Samarium (Si-Mag-Sm).

The samples were prepared following the modified Stöber method.[15-17] For the synthesis of Si-Mag-Sm particles, the following were added to a 1L capacity propropylene beaker: 640mL of ethanol (EXODO), 160mL of distilled water, 20mL of ammonium hydroxide (NEON), 4mL of tetraethyl orthosilicate - TEOS (SIGMA ALDRICH), 0.16g of iron oxide and 0.16g of samarium nitrate hexahydrate (SIGMA ALDRICH). The suspension was submitted to sonication for 20 minutes to allow the particles to achieve greater dispersion. Then the solution was submitted to magnetic stirring (IKA C MAG HS 7 stirrer) for 24 hours at room temperature, and the beaker surface was sealed with PVC film. After 24h, the particles formed were washed with distilled water and collected under the action of a magnet (plate of neodymium-iron-boron magnet with dimensions 10cm x 10cm x 2cm. They were then transferred to a petri dish. The samples were left in a humid atmosphere for 24h and then frozen and freeze-dried for 24h. The Si-Mag sample was obtained using the same procedure without the addition of samarium nitrate.

Theoretical neutron activation analysis method

Element ^{152}Sm is activated into ^{153}Sm when subjected to the process of neutron activation. In this process, a neutron source bombards neutrons on a sample containing ^{152}Sm atoms, and the sample may be activated into ^{153}Sm through the nuclear reaction n + ^{152}Sm is activated into $^{153}Sm \rightarrow {}^{153}Sm + \gamma$ accompanied by the decay $^{153}Sm \rightarrow \gamma + \beta + X$.

In order to perform the simulation of the radioactive activity of each chemical element in the sample as a function of its chemical concentration, a calculation was made for Neutron Activation Theoretical Analysis. The ideal activity of the chemical elements when submitted to a neutron beam, can be obtained from the following mathematical expression:[4-7]

$$A(t) = 0,6025.\frac{\omega.ma}{A}(\sigma_{ep}\phi_{ep} + \sigma_{th}\phi_{th}).(1 - e^{-\lambda.t}).e^{-\lambda.\delta} \quad (1)$$

In the expression, ω is the concentration of the element in the sample (%), *m* is the mass of the material to be activated (g); a is the isotopic abundance (%); *A* is the atomic mass (g) of the element; φth and φep represent the thermal and epithermal fluxes ($n.cm^{-2}.s^{-1}$), respectively; σth and σep represent the shock sections for thermal and epithermal neutrons (barns), respectively; λ is the disintegration constant expressed in s^{-1} ; *t* is the exposure time (s) of the material to the neutron flux and δ is the decay time after activation (s).

Characterization of the samples

Characterization of the iron oxide samples: A scanning electron microscopy (SEM) image was obtained on a Tescan Vega microscope. A secondary electron detector and a voltage of 20 mV were used to obtain high resolution images. A Transmission electron microscopy (TEM) was used because it is a widely used tool in the characterization of nanoparticles due to its high resolution and magnification capability. The resolution of an electron microscope can be as high as 0.1 nm if image aberrations or artifacts are minimized. The SEM tests were performed at Phosther Innovations and the MET at the Leibniz Institute for New Materials (INM) in Saarbrücken, Germany.

The Zeta potential of the iron oxide samples was analyzed in dispersion in deionized water. The dispersion was treated in an ultrasonic bath for 20 minutes. From the 60g of dispersion prepared, 18 mL were used for each titration, starting at the normal pH of the solution. At each pH 3 measurements were made, each consisting of 20 single measurements. The equipment used was the Zetasizer Nano ZSP from Malvern, the assays were performed at INM.

The samples were characterized by X-ray diffraction (XRD), in the Characterization and Microscopy Laboratory of CEFET-MG, using the Shimadzu XRD - 7000 diffractometer operating under the following conditions: CuKα radiation (35 KV/ 40 mA), goniometer speed 0.02° at 2θ per step, with standard counting time per step and collected from 5° to 80° at 2θ. The data were compared with standards contained in the PDF2 database (International Center for Diffraction Data - ICDD, 2003), X-Powder Ver. 2004.04.70 software, and backed up by examples found in the literature.

The 57Fe Mössbauer spectroscopy analyses were performed in a spectrometer at the Center for the Development of Nuclear Technology (CDTN) at the Federal University of Minas Gerais (UFMG), with constant acceleration, 57Co source in Rh matrix maintained at room temperature using transmission geometry. The Mössbauer system used at CDTN uses a transducer controlled by a linear function control unit and proportional counter type radiation detectors with a gas chamber with 97% Krypton and 3% CO2 at 1atm pressure. Spectra are taken at room temperature (RT) and quantitative analyses of the data are done using the Normos program. Isomeric shifts (IS) were standardized with respect to natural Fe (α-Fe).[10]

The magnetic properties of the samples were also evaluated at CDTN using a LakeShore model 7404 vibrating sample magnetometer. As a response to the VSM measurements, hysteresis curves were obtained, from which it is possible to obtain information about the magnetic properties of the analyzed material.

Characterization of silica particles containing iron oxide and samarium: The chemical composition of the samples was obtained by X-ray fluorescence using Shimadzu EDX-720 equipment. The analyses were performed under vacuum. The samples were characterized by X-ray diffraction (XRD), in the Characterization and Microscopy Laboratory of CEFET-MG, using the Shimadzu XRD - 7000 diffractometer operating under the following conditions: CuKα radiation (35 KV/ 40 mA), goniometer speed 0.02° at 2θ per step, with standard counting time per step and collected from 5° to 80° at 2θ. The data were compared with standards contained in the PDF2

database (International Center for Diffraction Data - ICDD, 2003), in the X-Powder Ver. 2004.04.70 software, and supported by examples found in the literature. The thermogravimetry test (TG/DTA) was performed on a Shimadzu DTG – 60H thermal analyzer. The test parameters were: heating rate 10ºC/min, maximum temperature 900°C, inert atmosphere with nitrogen and gas flow of 50ml/min. The chemical composition of the samples was also analyzed by means of Fourier Transform Infrared Spectroscopy (FTIR). For this, Shimadzu equipment was used, model IRPrestige-21 operated in ATR mode in the wavelength range of 4000 cm-1 a 400 cm-1 1 with a resolution of 4 cm-1.

Results and discussion

Iron oxide particles

SEM and MET images of the iron oxide sample used in the present work are shown in Figure 1.

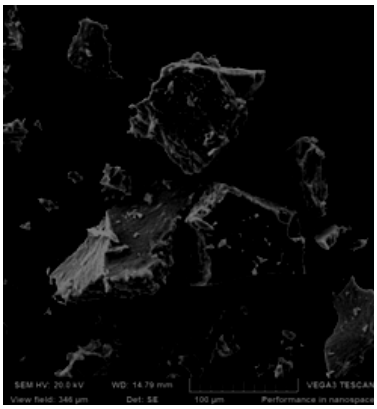

Figure 1 SEM and TEM image of naturel iron oxide.

Source: Phosther e INM.

It was observed by SEM that there is the formation of a particle aggregation (or clusters) of the iron oxides, of easy ultrasonic dispersion, i.e., the particles in the form of colloids are micrometric aggregates due to electrostatic interactions. It is also possible to distinguish from the TEM images that the particles are smaller than 15 nm, a size of interest in biomedical applications, primarily because of the controllable size on the order of a few nanometers, allowing interaction with cells (10-100µm), viruses (20-450 nm), proteins (5-50 nm) and genes (2 nm thick and 10-100 nm long). In addition the magnetic properties are of great interest as they allow manipulation by an external magnetic field gradient.[10]

Figure 2 shows the zeta potential results of the magnetite samples.

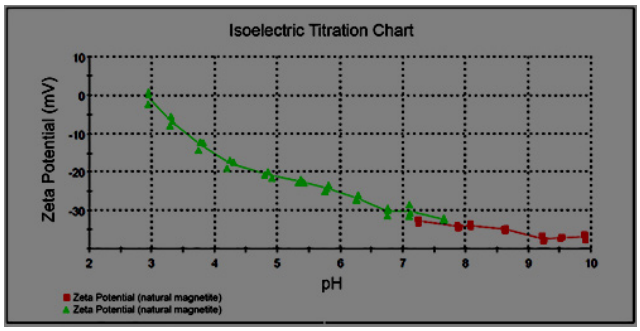

Figure 2 Zeta potential result of the iron oxide sample (natural magnetite).

Source: CEFET-MG [26]

The Zeta potential results of the samples indicate that the iron oxide particles exhibit good suspension stability in the physiological pH range (pH ~7) indicating that this material has excellent suspension properties for in vivo applications.

Figure 3 shows the diffractogram of natural and synthetic magnetite (produced by the coprecipitation route[10]).

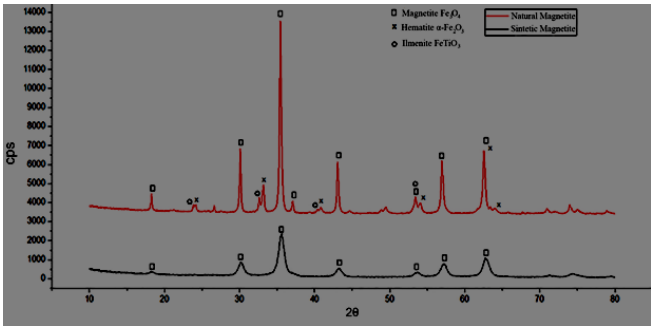

Figure 3 XRD of the natural and synthetic magnetite samples, insert with details regarding the peaks of the magnetite and maghemite phases.

Source: CEFET-MG [26].

Analyzing the diffractogram at room temperature, the peak at 57°, corresponding to the plane (511), highlighted in Figure 3, was selected, selecting the region between 55 and 60°. Two peaks are observed, at 57 and 57.5°, referring to the magnetite and maghemite phases, respectively.

The Mössbauer spectra obtained are shown in Figure 4 and Table 1. The synthetic magnetite sample was used for comparison with natural magnetite. The synthesized sample was produced by the coprecipitation route of Fe (II) and Fe (III) ions with ammonium hydroxide, in an inert nitrogen atmosphere, as described by Ferreira.[10]

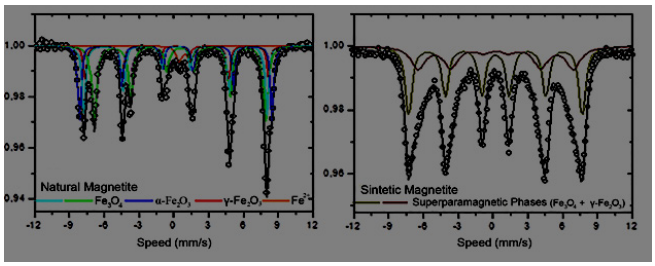

Figura 4 Result of the 57Fe Mössbauer spectrum of the iron oxide (natural magnetite) sample obtained at room temperature (RT).

Fonte: CDTN.

Table 1 Hyperfine parameters of the Mossbauer spectra of ^{57}Fe e obtained at RT

Sample	Phasis	δ ± 0,05 (mm/s)	Deq ± 0,05 (mm/s)	B_{HF} ± 0,5 (T)	Relative Area ±(1 %)
Natural Magnetite	α-Fe_2O_3	0,37	-0,17	51,4	18
	Fe_3O_4	0,65	0,01	45,8	43
		0,23	-0,02	48,9	21
	γ-Fe_2O_3 (*)	0,30	0,09	49,16	12
	$Fe_{1-x}O$	1,05	0,98	-	6

(*) Superparamagnetic behavior at RT

Source: CDTN.

Citation: Veloso G, Ferreira R, Roberto W, et al. Development of silica containing samarium and iron oxide for cancer treatment by brachytherapy and magnetic hyperthermia. *Int J Radiol Radiat Ther.* 2023;10(4):90–97. DOI: 10.15406/ijrrt.2023.10.00361

The results of the analyses by Mössbauer spectroscopy showed that the iron oxide (natural magnetite) sample presents a spectrum with narrow lines (or peaks) in comparison with other synthetic magnetite samples in the literature[10] that presents spectra with broad peaks, both are characteristics of iron oxides mixture with superparamagnetic behavior at room temperature.

The following oxides were identified in the natural sample: magnetite (Fe3O4) majority phase (64%), maghemite (γ-Fe2O3), hematite (α-Fe2O3) minority phases (12% and 18%, respectively) and traces of other oxides (6%). The technique provides values for the isomeric shift of the phases, relative to αFe, given by δ. In addition, values for the quadrupole unfolding (D) and the hyperfine magnetic field (Bhf) were also obtained.

The magnetization measurements of the natural material are presented in Figure 5 and compared with a synthetic magnetite.

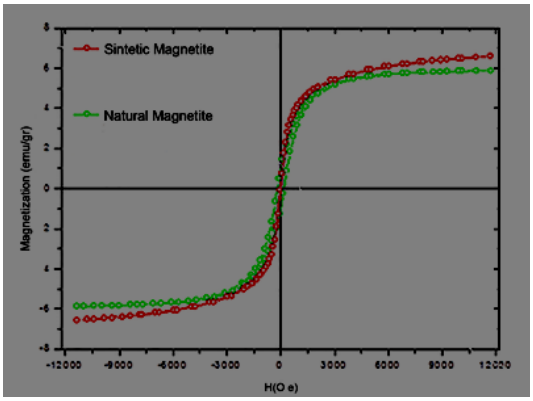

Figure 5 Magnetization measurements of natural and synthetic magnetite.

Source: CDTN.

The saturation magnetization values (σs) of both samples shown in Figure 5, are lower than those of standard non-nanostructured magnetite of the order of 92 emu/gr. However, the low saturation magnetization of these natural or synthetic magnetite samples may be associated with the ultrafine particles present. As a consequence of the surface area of these particles, the magnetic moments do not remain fully aligned and, therefore, the higher the surface area-volume ratio (smaller particle), the higher the contribution of unaligned moments and lower magnetization. In the case of natural magnetite, the low σs is due to the surface effect and the presence of other non-magnetic oxides, whose presence was also observed by XRD, shown in Figure 3, and Mössbauer spectroscopy. The high value of coercivity in natural magnetite can be attributed to the fraction of particles with sizes around 15 to 25 nm, whereas the coercivity close to zero in the case of synthetic magnetite may be associated with the slightly smaller particle size around 10 nm. The results show that both samples present low hysteresis loss, and very similar behavior under alternating electromagnetic field action.

The semi-quantitative results of chemical analysis by X-ray fluorescence spectroscopy (XRF) are presented in Table 2.

The Si-Mag and Si-Mag-Sm samples were analyzed by the XRF technique and the elementary percentage values were collected. The theoretical and experimental elemental proportions of Fe, Si and Sm obtained in the samples are shown in Table 3.

Table 2 EDX results of natural magnetite

Quantitative Result					
Analyte	**Result**	**Std.Dev.**	**Proc.-Calc**	**Line**	**Int.(cps/uA)**
Fe	91,437%	[0,205]	Quan-FP	FeKa	314,8208
Ti	5,244%	[0,056]	Quan-FP	TiKa	12,9544
Mn	0,880%	[0,017]	Quan-FP	MnKa	2,8479
Ca	0,865%	[0,021]	Quan-FP	CaKa	0,3075
P	0,648%	[0,116]	Quan-FP	P Ka	0,0153
S	0,319%	[0,046]	Quan-FP	S Ka	0,0273
V	0,302%	[0,021]	Quan-FP	V Ka	1,0495
Zn	0,116%	[0,013]	Quan-FP	ZnKa	0,2205
Cr	0,069%	[0,011]	Quan-FP	CrKa	0,2839
Nb	0,050%	[0,006]	Quan-FP	NbKa	0,3050
Zr	0,036%	[0,006]	Quan-FP	ZrKa	0,2052
Sr	0,033%	[0,006]	Quan-FP	SrKa	0,1595

Source: Phosther.

Table 3 Theoretical and experimental elemental compositions obtained by XRF analysis

	% Elementar Si-Mag		**% Elementar Si-Mag-Sm**	
Element	**Theoretical**	**Experimental**	**Theoretical**	**Experimental**
Fe	0.0173	88.775	0.0173	50.556
Si	0.0758	4.120	0.0757	40.652
Sm	-	-	0.0081	5.169
Ti	-	3.617	-	2.204
Mn	-	0.720	-	0.343
V	-	-	-	0.140
Al	-	-	-	0.936
Cr, Zr, Bi, Nb, Ba		2.768		-
Reagents	99.9069	-	99.8989	-
Total	**100**	**100**	**100**	**100**

Source: CEFET-MG.

It is observed that the natural magnetite sample presents elements other than iron oxides, such as titanium and manganese, probably from the mining process. The natural magnetite sample has more than 91% iron. Since this is a semi-quantitative analysis, it can be stated that the other elements found are traces or interferences of the technique.

Si-Mag and Si-Mag-Sm samples

The Si-Mag and Si-Mag-Sm samples were analyzed by the XRF technique and the percent elemental values were collected. The theoretical and experimental elemental ratios of Fe, Si, and Sm obtained from the samples are shown in Table 3.

The theoretical elemental percentage was obtained from the calculation of the elemental mass used in the experiment in relation to the total mass of the synthesis elements. Table 3 provides the information of the theoretical and experimental elemental percentages for each system so that the final elemental concentration of Fe, Si and Sm produced can be observed. The reactant elements used in the synthesis are: O, H, N, and C. The percentage of these was summed.

From the FRX elemental analysis it was possible to infer that there was synthesis of silica incorporated with samarium and iron oxide. Some impurities from the iron oxide sample were also incorporated into the system. Compared to the sample with samarium (Si-Mag-Sm), the Si-Mag sample showed an amount of silica around one tenth of the silica in Si-Mag-Sm, indicating that samarium seems to favor the production of core-shell structures in association with silica. In the presence of samarium nitrate there was a reduction in the amount of incorporated iron oxide (from 89% to 51%), which indicates that samarium seems to disfavor the incorporation of iron oxide into the coating.[10,14] This behavior needs to be further investigated.

X-ray diffractograms (XRD) were obtained for the Si-Mag and Si-Mag-Sm samples. The graph is shown in Figures 6.

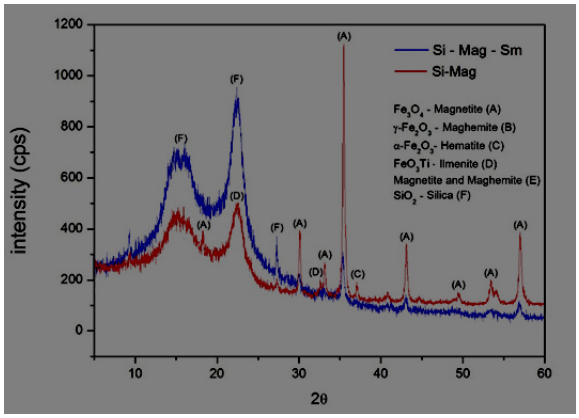

Figure 6 X-ray diffractogram for the Si-Mag sample.

Source: CEFET-MG

The X-ray diffractogram for the Si - Mag sample exhibited peaks from 5° to 23°, 18°, 30°,35.5°, 43°, 53°, 57°. The X-ray diffraction (XRD) analysis was compared with tabulated standards for magnetite (Fe3O4) (PDF 19-0629), maghemite (ϒ-Fe2O3) (PDF 39-1346) and hematite (α-Fe2O3) (PDF 87-1166), obtained from the PDF2 database. The diffractogram exhibits broad bands from 5° to 23° that refer to amorphous silica. Roberto et al.[5] also attributed this low intensity of crystalline peaks to the predominant amorphous characteristic of their sample obtained by Sol-Gel method.

Peaks 18°, 30°, 35.5°, 43°, 53°, 57° refer to the presence of magnetite, with 30.3°and 43.5° referring to the maghemite phase. Peak 33° indicates the presence of hematite. Peaks 23.9°and 32.5° verify the presence of ilmenite, a natural oxide of iron and titanium (FeTiO3) from titanium mining. The diffractogram of the Si-Mag sample shows that there has been formation of silica and incorporation of the iron oxide particles.

The diffractogram of the Si-Mag-Sm sample is shown in Figure 6.

The X-ray diffractogram for the Si-Mag-Sm sample exhibited peaks from 5° to 23°, 27.7°, 35.5°, 43°, and 57°. The diffractogram exhibits broad bands from 5° to 23° that refer to amorphous silica, as did the previous sample. The percentage of iron oxide in the sample showed a decrease upon incorporation of samarium nitrate into the complex, corroborated by the XRF technique. This behavior needs to be investigated. The expected samarium peaks between 13° and 31° were not observed indicating that these may be being convoluted by the amorphous halo, as a drop in crystallinity of the sample was observed, shown by the characteristic bands of silica formed. The diffractogram of Deepa et. al.[18] showed that borate glasses doped with samarium oxide exhibit a broad diffusion band at lower scattering angles, indicating the presence of long-range structural disorder that is characteristic of amorphous nature. Another reason for the absence of the peak. In addition considerable decrease in the intensities of the magnetite peaks was observed in the sample, and the subsequent appearance of the peak attributed to maghemite, which may be related to an oxidative process that occurred during the coating. This may also be related to the addition of samarium nitrate to the synthesis, indicating its influence on the iron oxides.

Infrared spectroscopy (FTIR) was used to characterize the Si-Mag and Si-Mag-Sm samples. Figure 7 displays the FTIR spectrum obtained for the Si-Mag sample.

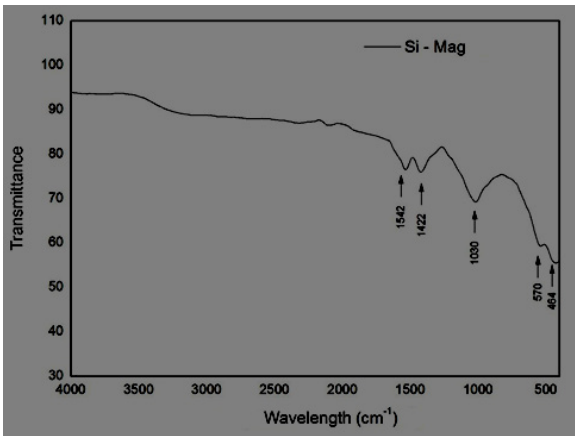

Figure 7 FTIR spectrum for the Si-Mag sample.

Source: CEFET-MG

The FTIR spectrum obtained for the silica sample containing iron oxides shows bands at 1542, 1422, 1030, 580 and 464 cm-1. The last two are confirmation of the presence of iron oxide in the sample, as they are associated with the Fe-O bonds. The other bands are associated with the presence of the silica particles formed. The silica is adsorbed onto the magnetite surface via Fe-O-Si bonds. The incorporation of the iron oxide on the silica particle can be confirmed by the presence of the band at 570 cm-1.[10] Such a band can be attributed to the vibration of the Fe-O bond of the Fe3O4 crystal structure. The vibrational mode 1030 cm-1 is part of the glassy network of the material formed by Si-O-Si bonds.[20] This evidences the formation of silica from its TEOS precursor. The bands in the range 1600 - 1400 cm-1 are related to the -OH functional group present on the surface of silica(OH) particles.[21,22]

Figure 8 displays the FTIR spectrum obtained for the Si-Mag-Sm sample.

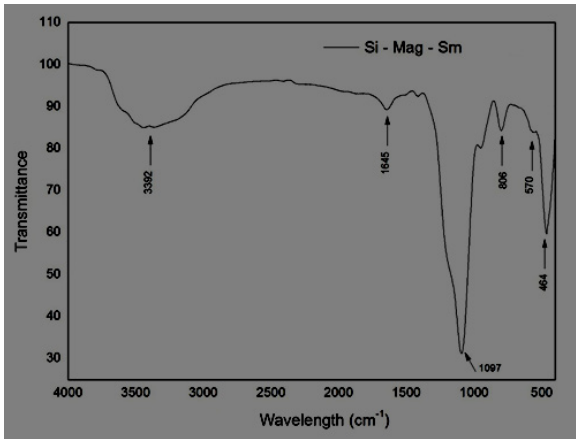

Figure 8 FTIR spectrum for the Si-Mag-Sm sample.

Source: CEFET-MG

The FTIR spectrum obtained for the silica sample containing magnetic and samarium particles exhibits bands at 3392, 1645, 1097, 806 and 580 and 464 cm^{-1}. The 464 cm^{-1} band assigned to the Fe-O bond confirms the presence of iron oxide in the structure of the obtained silica particle. A reduction of the 570 cm^{-1} band was observed, which, like the 464 cm^{-1} band, also appears in the spectrum of the Si-Mag sample. The band at 570 cm-1, analogously to the previous sample, is attributed to the Fe-O-Si bond. This reduction of the two bands can be attributed to the reduction in the concentration of iron particles incorporated into the sample due to the addition of samarium. This can be confirmed by the XRF results.

The 1097 cm-1 band is attributed to the Si-O-Si bond, as mentioned in the previous sample, which also evidences the formation of silica for this sample. In this region, approximately in the 1033 cm-1 range, the vibration referring to Sm+3 would also be observed.[18,24] However due to the higher proportion of silica present, there may be an interference of the Si-O-Si bond band in the samarium. The broad band at 3392 cm-1 attributed to stretching of -OH groups and the band at 1645 cm-1 attributed to deformation of the H-O-H bond suggest the existence of adsorbed water on the surface of the particles.[25]

Thermograms were obtained for the Si-Mag and Si-Mag-Sm samples. Figure 9 shows the thermogram obtained for the silica sample incorporated with iron oxides (Si-Mag).

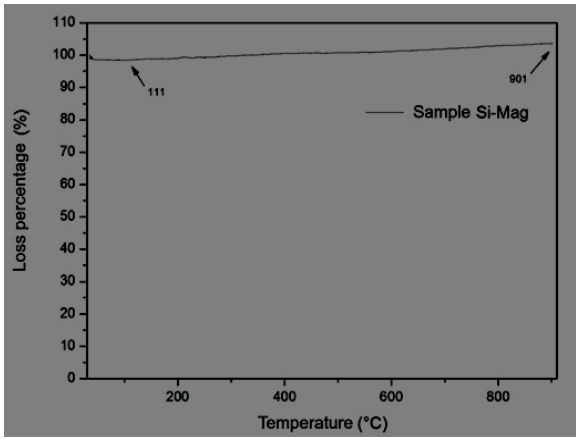

Figure 9 Thermal analysis of the Si – Mag sample.

Source: CEFET (2019)

The thermal analysis curve of the silica-coated iron oxide sample shows a mass gain. Initially, there is a mass reduction of about 1% in the range of 34°C to 111°C, which can be attributed to water and alcohol molecules adsorbed on the silica surface.[10]

The 11% mass gain in the temperature range between 111°C and 901°C indicates that possibly there was a mineralogical transformation analogous to that described for the Mag sample. However, the FRX analysis indicated that a low amount of silica was produced, unlike than expected by Ferreira.[10] The silica was not able to coat the oxide. This behavior needs to be investigated.

Residual mass was 103.8%.

Figure 10 shows the thermogram obtained for the Si – Mag - Sm sample.

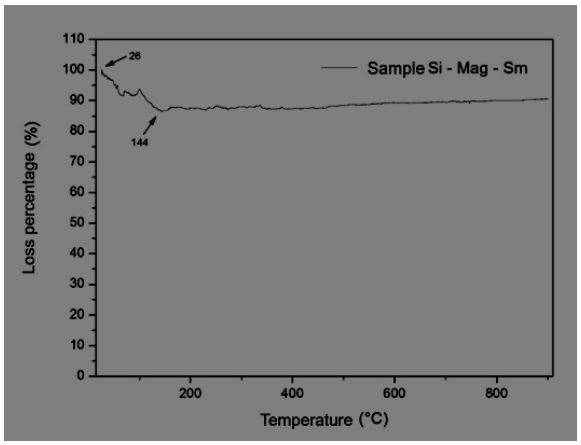

Figure 10 Thermal analysis of the Si – Mag - Sm sample.

Source: CEFET (2019)

The thermal analysis curve of the silica-coated iron and samarium oxides sample shows loss of mass. Initially, there is a mass reduction of 13% in the range of 26°C - 144°C, which can be attributed to water and alcohol molecules adsorbed on the silica surface.[10] According to the FRX analysis, the amount of silica formed was greater for this sample, which can be observed by a more pronounced mass loss attributed to alcohol molecules.

Also according to the FRX technique, only 5% of the element samarium was found in the sample, so it can be inferred that its incorporation into the system was low, and it was not possible to establish a direct relationship between its presence and the thermogram in question.

In the temperature range of 144°C – 901°C there is a mass gain of approximately 4.6%, which is similarly related to the mineralogical phenomenon described in the Mag sample. Residual mass was 90%.

Table 4 outlines the result of the initial and final activity calculation (after 24h) for the elements whose experimental elemental percentages were displayed in Table 3.

The elements Ti, Mn, V and Al are treated as impurities of the Si-Mag-Sm sample and their impacts were discarded due to the fact that they obtain physical characteristics such as half-life and shock sections considerably lower than those presented by ^{152}Sm. Through the activity calculation performed, it can be inferred that the other elements present would not present radioactive activity greater than the nuclide ^{153}Sm after 24 hours. It can be inferred that the element samarium is radioactively interesting for the purpose of the study, which offers favorable conditions for its continuation.

Tabel 4 Result of the initial and final activity calculation of the Si-Mag-Sm sample elements evidenced by the XRF technique

Parent Element	a (%)	σth barns	σep barns	Daughter Element	Half-Life	A* MBq.mg^{-1}.Φ $^{-1}$	A‡δ MBq.mg^{-1}.Φ $^{-1}$
^{54}Fe	5,8	2,252	1,32	^{55}Fe	2,73 a	1,15x10^{-9}	1,14x10^{-9}
^{58}Fe	0,28	1,149	1,23	^{59}Fe	44,503 d	2,06x10^{-11}	2,03x10^{-11}
^{56}Ti	5,4	0,178	0,14	^{57}Ti	5,76 min	4,45x10^{-10}	4,00x10^{-85}
^{144}Sm	3,1	1,63	1,902	^{145}Sm	430 d	2,26x10^{-12}	2,23x10^{-12}
^{152}Sm	26,7	206,2	2764,4	^{153}Sm	46,284 h	2,40x10^{-8}	1,68x10^{-8}
^{154}Sm	22,7	8,325	8,393	^{155}Sm	22,3 min	6,41x10^{-9}	4,67x10^{-28}
^{30}Si	3,1	0,1075	0,708	^{31}Si	157,3 min	4,97x10^{-8}	8,75x10^{-11}
^{55}Mn	100	13,41	13,3	^{56}Mn	2,579 h	2,32x10^{-8}	3,70x10^{-11}
^{51}V	0,14	4,9	4,8	^{52}V	3,743 min	1,22x10^{-8}	3,28x10^{-124}
^{27}Al	100	0,234	0,232	^{28}Al	2,241 min	8,38x10^{-17}	4,78x10^{-210}

***With irradiation time t=1h. ‡With decay time Θ=24h**

Conclusion

The natural iron oxide nanoparticles were characterized as received, showing that this sample is mostly natural magnetite (Fe3O4). The characterizations study of these particles also showed the presence of two other minority phases maghemite (γ-Fe2O3), hematite (α-Fe2O3), in addition to traces of other oxides (6%). The magnetic and morphological properties of these nanoparticles indicate that they have suitable characteristics for application as agents for magnetic hyperthermia.

The silica particles containing magnetic nanoparticles of iron and samarium oxides were obtained by the modified Stöber method. The formation of the particles containing silica, iron oxide and samarium were confirmed by FTIR, XRD and FRX. The Fe and Sm content in the Si-Mag-Sm sample was 51% and 5.1% respectively. The Si-Mag sample had 88% Fe. The drop in the percentage of Fe in the Si-Mag-Sm sample relative to the Si-Mag sample was an unexpected event and this behavior needs to be investigated.

The theoretical dosimetric study showed that the most interesting radioactive element for the purpose of the study is samarium. The Si-Mag-Sm sample will undergo neutron activation in order to prove in 153Sm the only possible sample element for application in brachytherapy, ruling out the hypothesis that the other elements present will have significant emissions capable of influencing the treatment when irradiated. With the use of samples synthesized with 152Sm in brachytherapy treatment, there will be a reduction in the activation time (neutron activation) of the material to obtain the same activity in relation to what is practiced in conventional procedures that use other radionuclides, making this process feasible for institutions that do not have nuclear reactors, but rather sealed neutron sources, which generally have lower neutron fluxes than nuclear reactors.

Acknowledgments

The authors thank to CEFET-MG for the scholarship granted during the period of this work, the Center for Development of Nuclear Technology (CDTN) and the Leibniz Institute for New Materials (INM) in Saarbrücken, Germany for the laboratory support for the development of this research. Our thanks to CNPq, CAPES and FAPEMIG (REMETTEC project) for the financial support, acquisition of equipment and supplies for the research. The authors thank to MSc, Gabriela Moreira Lana and Dr. Peter Oliveira (INM) and Dr. José Domingos Ardisson and Dr. Luis Fernandez-Outon (CDTN) for performing the sample characterization tests.

Conflicts of interest

All authors declare that there is no conflicts of interest.

References

1. WHO – World Health Organization. WHO report on cancer: setting priorities, investing wisely and providing care for all. Geneva: World Health Organization; 2020. Licence: CC BY–NC–SA 3.0 IGO.
2. IARC – International Agency for Research on Cancer. World Cancer Report: Cancer Research for Cancer Prevention. Geneva: World Health Organization; 2020. Licence: CC BY–NC–ND 3.0 IGO.
3. INCA – Instituto Nacional Do Câncer. Câncer: Estadiamento. Rio de Janeiro, SD.
4. Cember H, Johnson TE. Introduction to Health Physics, Mc Grow Hill, United States of America, 2009. p. 843.
5. Roberto WS, Pereira MM, Campos TPR. de. Structure and dosimetric analysis of biodegradable glasses for prostate cancer treatment. *Artificial Organs.* 2003;27(5):432–435.
6. Cember H. Introduction to Health Physics. 3rd ed. New York, Mc Graw Hill, 1989.
7. Chilton AB, Shultis JK, Faw RE. Principles of radiation shielding. Prentice–Hall, Inc, NJ–USA, 1984.
8. Allaf MA, Shahriari M, Sohrabpour M. Monte Carlo source simulation technique for solution of interference reactions in INAA experiments: a preliminary report. Radiation Physical Chemistry. 200469(6):461–465.
9. Delpino, GP, Borges R, Zambanini T, et al. Sol–gel–derived 58S bioactive glass containing holmium aiming brachytherapy applications: A dissolution, bioactivity, and cytotoxicity study. Materials Science and Engineering: C, 2021;111595.
10. Ferreira RV. Síntese e caracterização de nanopartículas magnéticas funcionalizadas com núcleo magnético de magnetita. Dissertação (Mestrado) – Universidade Federal de Minas Gerais. Departamento de Química. Belo Horizonte – MG, 2009.
11. Dönmez D, Elif C, Dönmez A. Magnetic hyperthermia for cancer treatment. Educational Sciences. 2020;50.
12. Pareta RA, Sirivisoot S. Calcium phosphate–coated magnetic nanoparticles for treating bone diseases. In: Nanomedicine: technologies and applications. *Woodhead Publishing.* 2012;49(6):131–147.
13. Gilchrist RK, Medal R, Shorey WD, et al. Selective inductive heating of lymphonodes. *Ann Surg.* 1957;146(4):596–606.
14. Mahmoudi M, Sant S, Wang B, et al. Superparamagnetic iron oxide nanoparticles (SPIONs): Development, surface modification and applications in chemotherapy. *Adv Drug Deliv Rev.* 2011;63(1–2):24–46.
15. Ebelmen M. *Ann Chimie Phys.* 1846;16:129.
16. Wright JD, Sommerdijk NAJM. Sol–gel materials chemistry and applications; London, Taylor & Francis; 2001.

17. Stöber W, Fink A, Bohn E. Controlled growth of monodisperse silica spheres in the micron size range. Journal of Colloid and Interface Science. 1968;26(1):62–69.

18. Deepa AV, Priya M, Suresh S. Influence of Samarium Oxide ions on structural and optical properties of borate glasses. *Academic Journals.* 2016;11:57–63.

19. Wang Y, Maramatsu A, Sugimoto T. FTIR analysis of well–defined α–Fe2O3 particles. Colloids and Surfaces A: Physicochemical and Engineering Aspects. 1998;134(3):281–297.

20. Hwa LG, Hwang SL, Liu LC. *Journal of Non–Crystalline*. Solids. 1998;238:193.

21. Moreira GF, Peçanha ER, Monte MBM, et al. XPS study on the mechanism of starch–hematite surface chemical complexation. *Minerals Engineering*. 2017;110:96–103.

22. Rubio F, Rubio J, Oteo JL. A FT–IR study of the hydrolysis of Tetraethylorthoselicate (TEOS). *Spectroscopy Letters.* 1998;31:199–219.

23. Ferraro RJ. The nitrate symmetry in metallic nitrates. *Journal of Molecular Spectroscopy.* 1960;4(1–6)*:*99–105.

24. Vratny F, Kokalas JJ. The reflectance spectra of metallic oxides in the 300 to 1000 Millimicron Region. *Applied Spectroscopy.* 1959;16(6):176.

25. Chanéac C, Tronc E, Jolivet JP. Magnetic iron oxide–silica nanocomposites. Synthesis and characterization. *Journal of Materials Chemistry.* 1996;12:1859–1969.

26. Lana GM. Aplicação de partículas magnéticas revestidas com fosfatos de cálcio para tratamento de câncer de ovário. Dissertação (Mestrado) – Centro Federal de Educação Tecnológica de Minas Gerais. Departamento de Engenharia de Materiais. Belo Horizonte – MG, 2018.